Semiconductors, 2024, Vol. 58, No. 12

Mechanisms of current transport in TiN/$Ge_2Sb_2Te_5$/Au structure

© S.A. Fefelov[1], L.P. Kazakova[1,2], N.A. Bogoslovskiy[1], A.B. Bylev[2]

[1] Ioffe Institute,
194021 St. Petersburg, Russia
[2] Kirov State Forest Technical University,
194021 St. Petersburg, Russia
E-mail: s.fefelov@list.ru

Received October 10, 2024
Revised December 27, 2024
Accepted January 16, 2025

The results of the study of $Ge_2Sb_2Te_5$ films of submicron thickness from 40 to 800 nm are presented. The current-voltage characteristics of TiN/$Ge_2Sb_2Te_5$/Au structures were measured and compared. It is established that the electrode resistance and the near-contact space charge region have a significant effect on the current-voltage characteristic. It is shown that the near-contact space charge region, located mainly in the $Ge_2Sb_2Te_5$ film, is the region where the switching process appears. The critical field strength at which the switching process in the space charge region begins is estimated. A method for determining the field strength in the amorphous part of the film before switching is proposed.

Keywords: chalcogenide glassy semiconductors, $Ge_2Sb_2Te_5$, phase-change memory, switching, contact resistance.

DOI: 10.61011/SC.2024.12.60383.7194

1. Introduction

In recent years, nonvolatile memory elements based on chalcogenide glassy semiconductors (CGS) have been produced. Such memory elements are called Phase Change Memory, or simply phase memory. Their operation is based on a significant difference in the conductive properties of chalcogenide semiconductor in the amorphous and crystalline states, as well as the fact that some CGS compositions, in particular $Ge_2Sb_2Te_5$ (GST225) can be quickly and repeatedly transferred from the amorphous state to the crystalline state and back by applying the appropriate current pulse. The amorphous and crystalline states themselves can be maintained for a long time without any additional energy consumption. Applied design solutions for phase memory elements are described, for example, in [1]. By choosing the parameters of current pulses partial crystallization of the substance in the memory cell can be achieved, which will allow the transition to multi-level data recording and a significant increase in the efficiency of phase memory cells [2]. Due to this, phase memory is also considered as a promising candidate for neuromorphic computing [3], since the ability to be in states with intermediate resistance values is an important requirement for artificial synapses. A description of both existing and promising applications of phase memory materials and methods for modifying CGS to obtain materials with suitable characteristics can be found, for example, in [4]. However, although the key properties of chalcogenide semiconductors — switching and memory effects — were discovered as early as the 1960s by Kolomiits and Lebedev [5], Pearson [6] and Ovshinsky [7], the physics of the processes occurring in CGS when current pulses are applied has not yet been fully understood. A discussion of the various mechanisms proposed to explain the switching and memory effects is given, for example, in [8]. Furthermore, the transition to submicron and, indeed, nanometer dimensions of the active region of CGS in phase memory elements requires special consideration of contact resistances, since they can affect the performance of memory devices. This issue has attracted the attention of researchers in recent years and has not yet been addressed [9,10]. The lack of an unambiguous description of the processes occurring in thin films of CGS when the current pulses are applied to them, slows down the development of manufacturing technologies and improvement of phase memory elements. Therefore, studying the specific features of current flow through thin films of CGS remains a relevant problem.

This paper provides the results of investigating GST225 films with submicron thicknesses from 40 to 800 nm. The current flowed in the transverse direction. When considering the current flow in the GST film, the influence of contacts was taken into account. The obtained data on the mechanisms of current flow in the near-contact space charge region (SCR) may be of interest to optimize the design parameters of phase memory elements.

2. Samples and experimental procedure

This study presents the results of investigating CGS films of CGS composition GST225 of different thicknesses when they are subjected to a series of triangular current pulses of increasing amplitude. Since the volt-ampere characteristic of CGS films usually has *S*-shaped character, the current strength was chosen as a controllable parameter in the experiment. The advantages of using a current generator in the measurement circuit were discussed in [11]. The studied samples had a „sandwich“ structure consisting of

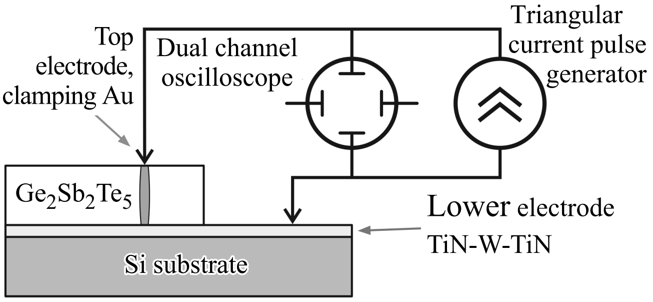

Figure 1. Diagram of the setup.

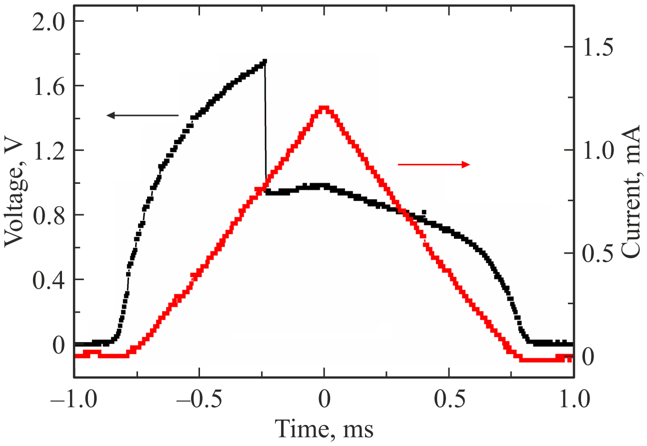

Figure 2. Synchronized oscillograms of the sample voltage and current pulse.

a thermally oxidized silicon substrate with a thickness of $\simeq 1$ mm (the SiO_2 oxide layer on the surface had a thickness of $\simeq 1\,\mu$m), further deposited on the substrate of the complex electrode layer with a total thickness of 100 nm (25 nm TiN, 50 nm W, 25 nm TiN), sputtered on top of the electrode GST225 film with thicknesses of 40, 130, 400 or 800 nm. A clamped gold electrode was used as the second electrode. The area of the film was $\simeq 1\,cm^2$. The top clamping electrode had a film contact area of $\simeq 10^{-4}\,cm^2$. The GST225 film was deposited by magnetron sputtering of a polycrystalline target. The composition and characteristics of the film were verified by Auger spectroscopy, energy dispersive X-ray spectroscopy, X-ray diffraction, X-ray phase analysis and transmission electron microscopy. It was found that the composition of the film was close to that of GST225 with homogeneous distribution of elements and the film was in an amorphous state [12,13].

Figure 1 shows a diagram of the measuring setup. The place of contact with the film of the upper clamping electrode could be changed. The current contact to the lower electrode was also clamped, but its position was fixed and was not changed further. At the same position of the upper clamping electrode, a sequence of triangular current pulses with increasing amplitude values was applied to the film. For control purposes, the pulse with a given amplitude value could be repeated. The maximum current value in the pulses varied from $6\,\mu$A to 8 mA, which covered the permissible range of currents and voltages that did not cause film destruction. The pulse duration was ~ 2 ms. Freshly sputtered films were investigated. Measurements were repeated at different points of the film surface, which allowed estimating the scatter in the values of parameters characterizing the current pulse passing through the film.

In Figure 2 synchronous oscillograms of voltage on the sample and current through the sample are presented as an example. Since the current varies linearly with time, the time axis on the oscillogram of voltage on the sample is actually the current axis and the voltage oscillogram actually immediately provides the volt-ampere characteristic (VAC) of the sample on the passing current pulse.

The oscillogram of voltage on the sample shown in Figure 2 shows a dramatic voltage jump (switching). The duration of the jump was not determined in the experiment. The record of voltages output to the digital oscilloscope was made with the step $\sim 1\,\mu$s.

The VACs obtained from the oscillograms consist of a part plotted along the rising branch of the current pulse and a part plotted along the falling branch of the current pulse. Thus, it is possible to compare the rising and falling branches of VAC of the same pulse, as well as the falling branch of the VAC of one pulse with the rising branch of the VAC of the next pulse.

3. Experimental results and discussion

In all cases, the rising branch of the VAC of the next pulse followed the falling branch of the previous pulse to the extent that the current forces coincided. Repeated application of a current pulse with the same amplitude value produced a VAC coincident with the falling branch of the VAC of the preceding pulse. The rising and falling branches of the VAC for a single pulse with a given current amplitude value applied for the first time could be different. If the current amplitude in the pulse was less than the threshold current amplitude, i. e., switching did not occur, the rising and falling branches of the VAC coincided. After the switching effect occurred, the sample resistance decreased when a current pulse with a higher amplitude was applied. The resistance of the sample after switching is determined by the amplitude of the current pulse applied to it.

According to the results of our measurements, the qualitative appearance of the VAC and the character of the change in the shape of the VAC plotted by the applied current pulses were the same for all the studied samples with films of all thicknesses.

Figure 3 shows a typical VAC for films of all thicknesses as an example of one of the VACs obtained on a sample with a film thickness of 800 nm. The black color shows the VAC measured at the switching pulse, the red color shows the VAC plotted from the current pulse following the switching pulse. The typical VAC parameters are marked:

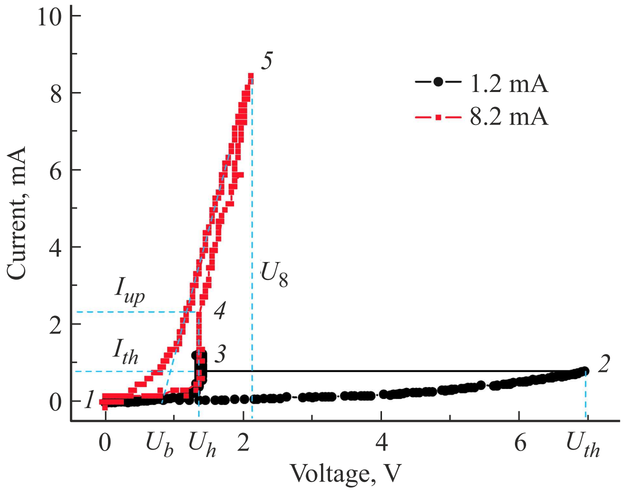

Figure 3. VAC for the 800 nm-thick film plotted using a current pulse with an amplitude of 1.2 mA (with switching) and a current pulse with an amplitude of 8.2 mA immediately following it.

U_{th} — switching voltage, I_{th} — switching current, U_h — support voltage, I_{up} — end current of the vertical region of the VAC, U_8 — voltage at a current of 8 mA, U_b — voltage characterizing the rectilinear part of the VAC for the incident branch of the current pulse of 8 mA.

When the current pulses are first applied with increasing amplitude, starting from a minimum amplitude of 6 μA, until the current in the pulse exceeds the switching current I_{th}, the rising and incident branches of the VAC follow the *1–2* region. When U_{th} is reached, a switchover occurs, the voltage drops sharply to U_h, and then a vertical region *3–4* usually follows in the VAC. The VAC corresponding to the falling branch of the current pulse at which switching occurred follows the line *4–3–1*. If the amplitude value of the next pulse does not exceed I_{up}, the corresponding rising and incident branches of the VAC generally follow the *1–3–4* region. As the current in the pulse is further increased, the VAC moves to the *4–5*, region, the rising and falling branches of the VAC are now different. Finally, a partially rectilinear VAC *1–5* is formed, which can be characterized by the voltage U_b and differential resistance R_d for the rectilinear region. The values of all these quantities have some spread depending on the position of the top clamping electrode on the film surface. The average values of these parameters for ten points are given in the table for films of different thicknesses.

It should be noted that the vertical region *3–4* on the VAC is practically absent for a 40 nm thick GST film, and the thicker the film, the longer the vertical region. The table also shows the surface-averaged voltages for currents of 6 and 100 μA for the *1–2* region on the VAC.

Let us consider the region *1–5* on the VAC of the samples. According to the data provided in the table, the voltage U_8 at a current $I = 8$ mA is practically independent of the film thickness for samples with films of thickness 40, 400, and 800 nm. Since the incident branch of the VAC (region *5–1*) for this current pulse is almost straight in its upper part and its slope is also weakly dependent on the film thickness, it means that the film resistance in this region of the VAC makes almost no contribution to the total sample resistance, and R_d can be considered as an estimate for the electrode resistance (≈ 200 ohm). For the sample with 130 nm film, the resistance determined from the slope of the VAC in the *5–1* region was found to be ~ 100 Ohm, which is due to the different thickness of the bottom electrode in this sample. The difference in the values of the electrode resistances of the samples (100 and 200 Ohms) fully explains the difference in the U_8 voltage for the sample with the 130 nm film from the U_8 voltages for the other samples in the table. In fact, for the upper part of the *5–1* portion of the VAC, because of its straightness, $U \approx U_b + IR_d$ (see Figure 3). If the electrode resistance for the sample with 130 nm film was also ~ 200 Ohm, we would get U_8 V instead of 1.29 V for the $U_8 \approx 0.47 + 8.0 \cdot 10^{-3} \cdot 200 = 2.07$ voltage of this sample (see the table), which corresponds well to the U_8 voltages of the other samples. This agreement provides further confirmation that for the *1–5* regions on the VAC of the samples, the film is already in the crystalline state and makes a very small contribution to the resistivity of the samples. The initial part of the *1–5* region on the VAC is due to the barrier properties of the contacts, as discussed later.

Let us discuss the *1–2* region on the VAC of the samples. In this region, the GST film is still in the amorphous state. At a current of 6 μA, the voltage for the 40 nm film is 0.45 V, which corresponds to a sample resistance of 75 kOhm at an average field strength in the film of $\sim 10^5$ V/cm. Taking into account the evaluation of the electrode resistance, such a large sample resistance should be due to the GST film. In [14] for similar films, the resistivity value $\rho = 2.8 \cdot 10^4$ Ohm $\cdot$ cm was obtained for room temperature and field strength 10^3 V/cm, and the resistivity decreased with increasing temperature and field strength. If we assume the cross-region of the current channel to be equal to the contact area of the upper clamping electrode (10^{-4} cm^2), then for a 40 nm thick film, the film resistance will be ≤ 1 kOhm. Thus, it should be assumed that the resistance of this sample (40 nm thick) is mainly related to the contact

Parameters of the volt-ampere characteristics

GST film thickness	40 nm	130 nm	400 nm	800 nm
U, V at $I = 6\,\mu$A	0.45	0.47	0.53	0.64
U, V at $I = 100\,\mu$A	1.02	1.53	2.34	3.27
U_{th}, V	1.41	1.89	6.94	7.49
I_{th}, mA	0.40	0.27	1.09	0.49
U_h, V	0.75	0.82	1.18	1.59
U_8, V at $I = 8$ mA	2.18	1.29	2.05	2.15
U_b, V	0.50	0.47	0.70	0.84
R_d, kOhm	0.21	0.10	0.18	0.15

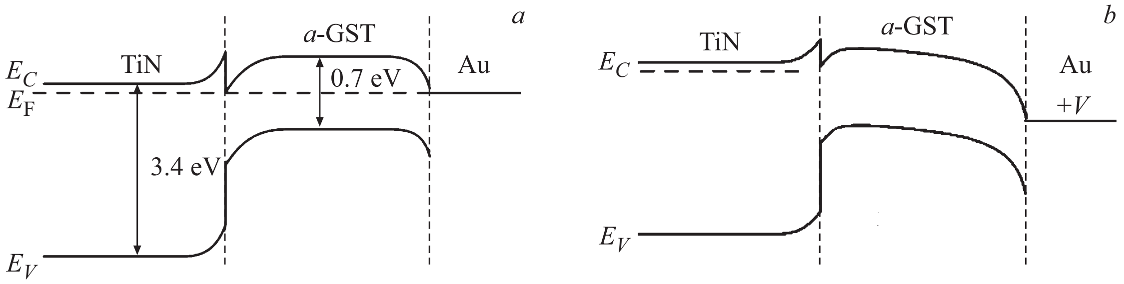

Figure 4. Energy diagram of the TiN/a-GST225/Au: a — structure: a — no applied voltage, b — positive potential on Au.

area of the film with the electrodes. On the other hand, it is generally recognized that CGSs have a high density ($\sim 10^{19}\,\mathrm{cm}^{-3}$) of defects of various kinds that form traps for charge carriers. Such states can lead to the appearance of surface potential barriers of blocking type. The formation of blocking barriers on metal-CGS contacts was experimentally confirmed for different CGS [15,16] compositions, and the barrier size was weakly dependent on the metal yield work. The Schottky barrier at the TiN/GST contact was discussed in [17]. Figure 4 schematically shows the energy diagram of the TiN/a-GST225/Au structure, in which it is taken into account that amorphous GST225 is a semiconductor with a predominant hole conduction type and a bandgap width of ~ 0.7 eV [18,19], TiN — a wide bandgap n-type semiconductor with a bandgap width of ~ 3.4 eV and a high concentration of charge carriers [20,21].

During our experiments, „plus" was applied to the gold electrode. If we consider GST225 to be a p-type [18,19] semiconductor, the contact (a-GST225/Au) is inversely shifted when an external voltage is applied in this way. As the applied voltage increases, the area of space charge arising at this contact, mainly on the film side, expands into the film. The TiN/a-GST225 contact, on the other hand, is directly displaced. According to the energy diagram of this contact, the current through the sample will be mainly due to recombination of electrons and holes at recombination centers, which can be numerous defects in the GST film. As the voltage increases, the electron flow through the conduction band will also contribute to the current. Thus, the field in the GST film is highly inhomogeneous and in the near-contact regions will be larger than in the film volume. These considerations are consistent with the conclusion that the main contribution to the sample resistance is made by the film region near the contacts.

Additional confirmation of the above situation is provided by the dependence of the voltage on the samples on the film thickness. Figure 5 shows the voltages on the samples at currents of 6 and 100 μA depending on the film thickness for the region *1–2* of the VAC (data from the table).

At a current of 6 μA, a linear dependence of voltage on thickness is observed. This linear dependence can be explained as follows, assuming that the temperature of the samples is the same regardless of the film thickness. The field in the films at a constant and identical temperature in all samples will be determined only by the current, and the SCR dimensions will not depend on the film thickness. If U_c — the voltage across the contacts, E_f — the field strength in the film volume, l — the film thickness, l_c — the SCR size, then the voltage across the sample can be represented as $U = U_c + E_f(l - l_c)$, which gives a linear dependence U on l, and the field strength in the film volume E_f determines the slope of this straight line. From the diagram we obtain $E_f = 2.5 \cdot 10^3\,\mathrm{V \cdot cm}$. Given the value of the current density $j = \frac{I}{S} = \frac{6 \cdot 10^{-6}}{10^{-4}} = 0.06\,\mathrm{A/cm}^{2}$ we find the resistivity of the film material $\rho = 4 \cdot 10^4\,\mathrm{Ohm \cdot cm}$, which agrees with the result obtained in [14]. This agreement also justifies the temperature assumption made, the sample temperature being — room temperature. At low currents due to the good heat dissipation of the sample, the role of temperature is apparently insignificant.

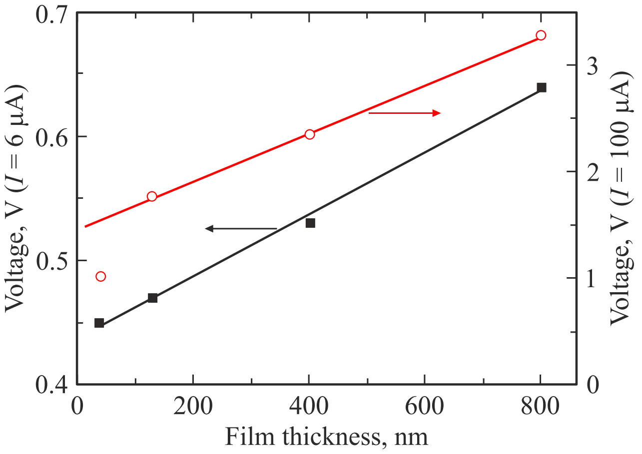

Figure 5. Dependence of the voltage on the sample on the film thickness at currents of 6 and 100 μA.

At a current of 100 μA, a linear dependence of voltage on thickness is also observed if we do not consider the sample with a film thickness of 40 nm. This can be explained by the fact that in the sample with a film thickness of 40 nm, the SCR has spread over almost the entire film thickness. In other films, the field strength in the film volume at this current, as follows from the graph, will be $E_f = 2.3 \cdot 10^4\,\mathrm{V \cdot cm}$, and the resistivity —

$\rho = 2 \cdot 10^4$ Ohm $\cdot$ cm. As can be seen, as the field increases, the resistivity of the film material decreases in agreement with the data given in [14] although this drop is somewhat smaller than in [14].

Switching currents for films of all thicknesses in our case exceeded $100\,\mu$A. For a sample with a thickness of 40 nm, at such currents, the SCR extends over the entire thickness of the film, and the processes that initiate switching occur in this region. Since the qualitative appearance of the SCR and the character of the change in the shape of the SCR, as mentioned above, are the same for samples with films of all thicknesses, it can be concluded that for films of other thicknesses, switching occurs in the SCR of the GST225/Au contact. Analysis of the VAC in the *1–2* region in the immediate vicinity of the switching voltage gives a dependence of the form $I \sim U^m$, where the value of m is in the range *4–6* for a 40 nm thick film and drops to 3–4 as the film thickness increases. This may indicate a „soft breakdown“ preceding the switching. The decrease of m as the film thickness increases may be due to an increase in the contribution of the film array to the stress on the sample. Various hypotheses about the nature of the switching process itself have been suggested [8], but a strong viewpoint on this subject has not been reached yet.

Taking into account the above discussion, the field strength in the SCR during switching can be estimated. According to the above discussion, the SCR occupies the entire film thickness for a sample with a thickness of 40 nm. We take (a-GST/Au) $\varphi_b = 2/3\ E_g/e \approx 0.5$ V as an estimate of the height of the surface potential contact barrier. Adding the value of U_{th} from the table, we find $E_{th} = \frac{U_{th} + \varphi_b}{l} \approx 5 \cdot 10^5$ V/cm.

Since in our case the switching was accompanied by an irreversible change in the VAC, the transition to the *1–3–4* region, we can conclude that the switching process also resulted in a restructuring of the film material structure, its transition to a metastable FCC crystalline phase in the region where the switching process developed.

The interpretation of the *3–4* region on the VAC depends on the chosen switching model. In any case, there seems to be an expansion of the film region in the crystalline state.

As for the *4–5* region of the VAC, taking into account the straightness for the same currents of the *1–5* region, as noted above, the contribution to the resistance of the electrode sample at the gradual final transition of the film into a low-resistance crystalline state becomes the determining factor in this VAC region. After that, the VAC is reduced to the *1–5* region, which is caused practically only by the electrodes, and the nonlinearity of the VAC in the initial region is associated with the potential barrier for electrons at the TiN/GST contact and the barrier for holes at the c-GST/Au boundary, which blocks the TiN side. The contribution of these barriers can be estimated by the parameter U_b on the VAC.

The spread of the parameter values characterizing the VAC obtained for different points of current pulse delivery on the surface of the samples can be related to the variable height of potential blocking barriers on the film surface due to the amorphous structure of the film.

4. Conclusion

The research method based on the use of triangular current pulses applied to samples with different film thicknesses of chalcogenide glassy semiconductor (GST225) allowed to determine that there are blocking potential barriers at the contacts GST/Au and TiN/GST. It was found that the electrode resistance and the near-contact region of space charge have a significant effect on the VAC. It is shown that the SCR of these contacts, located mainly in the GST film, is the region where the switching process develops. An estimation of the critical field strength at which the switching process begins in the SCR is given. A method for determining the field strength in the array of the amorphous part of the film before switching is proposed.

Conflict of interest

The authors declare that they have no conflict of interest.

References

[1] G.W. Burr, M.J. Breitwisch, M. Franceschini, D. Garetto, K. Gopalakrishnan, B. Jackson, B. Kurdi, C. Lam, L.A. Lastras, A. Padilla, B. Rajendran, S. Raoux, R.S. Shenoy. J. Vac. Sci. Technol. B, **28** (2), 223 (2010).

[2] G.W. Burr, M.J. Brightsky, A. Sebastian, H.-Y. Cheng, J.-Y. Wu, S. Kim, N.E. Sosa, N. Papandreou, H.-L. Lung, H. Pozidis, E. Eleftheriou, C.H. Lam. IEEE J. Emerg. Select. Top. Circuits Syst., **6** (2), 146 (2016).

[3] G.W. Burr, R.M. Shelby, A. Sebastian, S. Kim, S. Kim, S. Sidler, K. Virwani, M. Ishii, P. Narayanan, A. Fumarola, L.L. Sanches, I. Boybat, M. Le Gallo, K. Moon, J. Woo, H. Hwang, Y. Leblebici. Adv. Phys.: X, **2** (1), 89 (2017).

[4] S.A. Kozyukhin, P.I. Lazarenko, A.I. Popov, I.L. Eremenko. Uspekhi khimii **91** (9), RCR5033 (2022). (in Russian).

[5] B.T. Kolomiets, E.A. Lebedev. RE, **8** (12), 2097 (1963). (in Russian).

[6] A.D. Pearson, W.R. Northover, J.F. Dewald, W.F. Peck, jr. *Advances in Glass Technology* (Plenum Press, N.Y., 1962) p. 357.

[7] R.S. Ovshinsky. Phys. Rev. Lett., **21**, 1450 (1968).

[8] N.A. Bogoslovskiy, K.D. Tsendin, FTP, **46** (5), 577 (2012). (in Russian).

[9] R. Huang, K. Sun, K.S. Kiang, R. Chen, Y. Wang, B. Gholipour, D.W. Hewak, C.H. De Groot. Semicond. Sci. Technol., **29** (9), 095003 (2014).

[10] K.A. Cooley, H.M. Aldosari, K. Yang, S.E. Mohney. J. Vac. Sci. Technol. A, **38**, 050805 (2020).

[11] S.A. Fefelov, L.P. Kazakova, S.A. Kozyukhin, K.D. Tsendin, D. Arsova, V. Pamukchieva. ZhTF, **84** (4), 80 (2014). (in Russian).

[12] A.A. Sherchenkov, S.A. Kozyukhin, N.I. Borgardt, P.I. Lazarenko, A.V. Babich, A.O. Yakubov, D.Y. Terekhov, Y.S. Zybina. Sb. tr. Mezhdunar.conf. SPb, 2018), p. 83. (in Russian).

[13] A.O. Yakubov, A.A. Sherchenkov, A.V. Babich, P.I. Lazarenko, D.Yu. Terekhov. Sb. tr. Mezhdunar.conf. SPb, 2018), p. 96. (in Russian).
[14] A.A. Sherchenkov, S.A. Kozyukhin, P.I. Lazarenko, A.V. Babich, N.A. Bogoslovsky, I.V. Sagunova, E.N. Redichev. FTP, **51** (2), 154 (2017). (in Russian).
[15] D.I. Ciulianu. FTP, 22 (7), 1181 (1988). (in Russian).
[16] E.A. Senokosov, V.G. Surinov, V.S. Feshchenko, V.I. Chukita. Uspekhi prikl. fiziki, **8** (4), 273 (2020). (in Russian).
[17] R.-G. Nir-Harwood, G. Cohen, A. Majumdar, R. Haight, E. Ber, L. Gignac, E. Ordan, L. Shoham, Y. Keller, L. Kornblum, E. Yalon. ACSNano, **18**, 8029 (2024).
[18] T. Kato, K. Tanaka. Jpn. J. Appl. Phys., **44** (10), 7340 (2005).
[19] H. Tong, Z. Yang, N. Yu, L. Zhou, X. Miao. Appl. Phys. Lett., **107** 082101 (2015).
[20] M.N. Solovan, V.V. Brus, P.D. Maryanchuk. FTP, **47** (9), 1185 (2013). (in Russian).
[21] I.G. Orletsky, M.I. Ilashchuk, V.V. Brus, P.D. Maryanchuk, M.N. Solovan, Z.D. Kovalyuk. FTP, **50** (3), 339 (2016). (in Russian).

Translated by J.Savelyeva